Supplementary Information

Voltage dependent photoluminescence and how it correlates to the fill factor and open-circuit voltage in perovskite solar cells

Martin Stolterfoht[1,*], Vincent M. Le Corre[2], Markus Feuerstein[1], Pietro Caprioglio[1,3], L. Jan Anton Koster[2], Dieter Neher[1,*]

[1]Institute of Physics and Astronomy, University of Potsdam, 14476 Potsdam, Germany

[2]Zernike Institute for Advanced Materials, University of Groningen, Nijenborgh 4, 9747 AG, Groningen, Netherlands.

[3]Young Investigator Group Perovskite Tandem Solar Cells, Helmholtz-Zentrum Berlin für Materialien und Energie GmbH, Kekuléstraße 5, 12489 Berlin, Germany

email: stolterf@uni-potsdam.de, neher@uni-potsdam.de

Supplementary Methods:

Absolute Photoluminescence Measurements: Excitation for the PL imaging measurements was performed with a 445 nm CW laser (Insaneware) through an optical fibre into an integrating sphere. The intensity of the laser was adjusted to a 1 sun equivalent intensity by illuminating a 1 cm^2-size perovskite solar cell under short-circuit and matching the current density to the J_{SC} under the sun simulator (~22.0 mA/cm^2 at 100 mWcm^{-2}, or 1.375x10^{21} photons $m^{-2}s^{-1}$). A second optical fiber was used from the output of the integrating sphere to an Andor SR393i-B spectrometer equipped with a silicon CCD camera (DU420A-BR-DD, iDus). The system was calibrated by using a halogen lamp with known spectral irradiance, which was shone into to integrating sphere. A spectral correction factor was established to match the spectral output of the detector to the calibrated spectral irradiance of the lamp. The spectral photon density was obtained from the corrected detector signal (spectral irradiance) by division through the photon energy (hf), and the photon numbers of the excitation and emission were obtained from numerical integration using Matlab. In a last step, three fluorescent test samples with high specified PLQY (~70%) supplied from Hamamatsu Photonics where measured where the specified value could be accurately reproduced within a small relative error of less than 5%.

Voltage dependent PL measurements: The samples were illuminated outside the optical sphere in front of the detector using the same equipment as specified above for the absolute PL measurements. The samples were masked (4.32 mm^2) to ensure that only the active pixel was illuminated which has a size of 6 mm^2 without the mask. This is important to prevent emission from regions on the substrate which are outside of the active pixel and therefore not connected to the electrical circuit and consequently always under open-circuit conditions. The emitted PL from the sample was focused through optical lenses onto the detector. The relative PL yield was measured by varying the applied voltage to the cell starting from 0 V to 2 V in steps of 50-100 mV (using a Keithley 2400 SMU). The samples were held for ~10 s at each voltage to record the PL spectra while the cell was constantly illuminated during the sweep. The measured relative PL under open-circuit conditions was normalized to the PLQY at V_{OC} which was separately measured using the absolute PL setup.

Numerical drift-diffusion simulations: The simulations were performed using SCAPS which is an open-source code and can be obtained from https://users.elis.ugent.be/ELISgroups/solar/projects/scaps upon the conditions requested by the developers Marc Burgelman et al. Simulation parameters are shown below in **Supplementary Table S1**.

Device Fabrication: Pre-patterned 2.5x2.5 cm^2 15 Ω/sq. ITO substrates (Automatic Research, Germany) were cleaned with acetone, 3% Hellmanex solution, DI-water and iso-propanol, by sonication for 10 min in each solution. After a microwave plasma treatment (3 min, 200 W), the samples were transferred to a N_2-filled glovebox. For the *p-i-n*-type cells shown in the main text, PTAA (Sigma-Aldrich) layer with thickness of 8 nm, 40 nm and 85 nm were spin coated from a 1.5, 7.1 and 10 mg mL^{-1} PTAA/toluene solution at 6000 rpm for 30 seconds, 1000 rpm for 45 seconds and 500 rpm for 200 seconds, respectively. After 10 min annealing on a hotplate at 100 °C, the films were cooled down to room temperature and a 60 µL solution of PFN-Br (1-Material, 0.5 mg/mL in methanol) was deposited onto PTAA while the substrate was being spun at 5000 rpm for 20 s resulting in a film with thickness below the detection limit of our AFM (< 5 nm). No further annealing occurred. The doped PTAA layer was cast from a 7.1 mg mL^{-1} solution of PTAA:F4TCNQ (9:1 by weight) in toluene at 1000 rpm for 45 seconds. No annealing occurred.

The triple cation perovskite precursor solution was prepared from a 960 μL DMF:DMSO solution (4:1 by volume) including 1 M FAI (Dysol), 1.1 M PbI_2 (TCI America), 0.2 M MABr (Dysol), 0.2 M $PbBr_2$ (TCI America) mixed with 1.5 M CsI (Sigma Alldrich) in 40 μL DMF:DMSO (4:1 by volume). The perovskite layer was deposited by spin-coating at 4000 rpm for 35 seconds using an acceleration of 1333 rpm/s. After 10 seconds, 300 μL ethylacetate was dropped onto the spinning substrate for approximately 1 second (the anti-solvent was placed in the center of the film). The perovskite film was then annealed at 100 °C for 1 hour on a preheated hotplate. The samples were then transferred to an evaporation chamber where fullerene-C_{60} (30 nm), 2,9-Dimethyl-4,7-diphenyl-1,10-phenanthroline BCP (8 nm) and copper (100 nm) were deposited under vacuum (p = 10^{-7} mbar).

For the *n-i-p*-type cells shown in the Supporting Information, the substrates were cleaned as above. First, a 0.05% solution of ethoxylated-polyethylenimine (PEIE) in 2-Metoxyethanol was cast in air at 5000 rpm for 45 seconds atop the substrates, resulting in a film thickness below the detection limit of the AFM setup (< 5 nm). Then the substrates were transferred to the evaporation chamber to deposit a 30 nm C_{60} layer (as specified above). Afterward the perovskite layer was spun cast as detailed above. As HTL, undoped P3HT layer with different thicknesses were cast for 45 s from a dichlorobenzene (DCB) solution using the following concentrations and spin speeds: 12.5 mg mL^{-1} at 2000 rpm, 12.5 mg mL^{-1} at 1000 rpm and 25 mg mL^{-1} at 1000 rpm, which resulted in a film thickness of 35 nm, 80 nm and 150 nm, respectively. Finally, the *n-i-p* cells were completed by evaporating MoO_3 (8 nm) and Cu (100 nm) in vacuum (p = 10^{-7} mbar).

Supplementary Table S1. SCAPS simulation parameters.

Parameter	Symbol	Value	Unit
Majority carrier band offset between perovskite and C_{60}	$\Delta E_{\mathrm{maj,c}}$	0	eV
Majority carrier band offset between perovskite and PTAA	$\Delta E_{\mathrm{maj,v}}$	0	eV
Lifetime in perovskite	τ_{pero}	400	ns
Bimolecular recombination rate constant in perovskite	k_2	6x10^{-11}	cm^3s^{-1}
Lifetime in PTAA	τ_p	1	ns
Lifetime in C_{60}	τ_n	1	ns
Ionized acceptors in PTAA	$N_{\mathrm{A},p}^-$	0	cm^{-3}
Ionized donors in C_{60}	$N_{\mathrm{D},n}^+$	0	cm^{-3}
Intrinsic carrier density in perovskite	N_{i}	1x10^{10}	cm^{-3}
Minority carrier recombination velocity from perovskite to PTAA	$S_{\mathrm{min},n}$	200	cm/s
Minority carrier recombination velocity from perovskite to C_{60}	$S_{\mathrm{min},p}$	2000	cm/s

Majority carrier recombination velocity from perovskite to PTAA	$S_{\mathrm{maj},p}$	1x10^{7}	cm/s
Majority carrier recombination velocity from perovskite to C_{60}	$S_{\mathrm{maj},n}$	1x10^{7}	cm/s
Majority and Minority carrier velocity at front metal contact (ITO)	S_{met}	1x10^{7}	cm/s
Majority and Minority carrier velocity at back metal contact (Cu)	S_{met}	1x10^{7}	cm/s
Thickness of PTAA	d_{PTAA}	8 – 85	nm
Thickness of perovskite	d_{pero}	400	nm
Thickness of C_{60}	d_{C60}	30	nm
Offset between metal and PTAA	$\Delta E_{\mathrm{F,\,metal}-p}$	0.15	eV
Offset between metal and C_{60}	$\Delta E_{\mathrm{F,\,metal}-n}$	0.15	eV
Device built-in voltage	V_{BI}	1.3	V
Bandgap PTAA	$E_{\mathrm{G,PTAA}}$	3.0	eV
Electron affinity PTAA	$E_{\mathrm{A,PTAA}}$	2.5	eV
Bandgap perovskite	$E_{\mathrm{G,pero}}$	1.6	eV
Electron affinity perovskite	$E_{\mathrm{A,pero}}$	3.9	eV
Bandgap perovskite	$E_{\mathrm{G,pero}}$	2.0	eV
Electron affinity C_{60}	$E_{\mathrm{A,C60}}$	3.9	eV
Bandgap C_{60}	$E_{\mathrm{G,C60}}$	2.0	eV
Electron mobility in C_{60}	$\mu_{n,\,\mathrm{PTAA}}$	1x10^{-2}	cm^2/Vs
Hole mobility in PTAA	$\mu_{p,\,\mathrm{PTAA}}$	1x10^{-4}	cm^2/Vs
Electron mobility in perovskite	$\mu_{n,\,\mathrm{pero}}$	10	cm^2/Vs
Hole mobility in perovskite	$\mu_{p,\,\mathrm{pero}}$	10	cm^2/Vs
relative dielectric constant PTAA	ϵ_{PTAA}	3.5	
relative dielectric constant perovskite	ϵ_{pero}	70	
relative dielectric constant C_{60}	ϵ_{C60}	5.0	
Effective electron density of states in HTL	$N_{\mathrm{C/V,\,PTAA}}$	1x10^{20}	cm^{-3}
Effective electron density of states in C_{60}	$N_{\mathrm{C/V,C60}}$	1x10^{20}	cm^{-3}
Effective electron density of states in perovskite	$N_{\mathrm{C/V,pero}}$	3x10^{18}	cm^{-3}

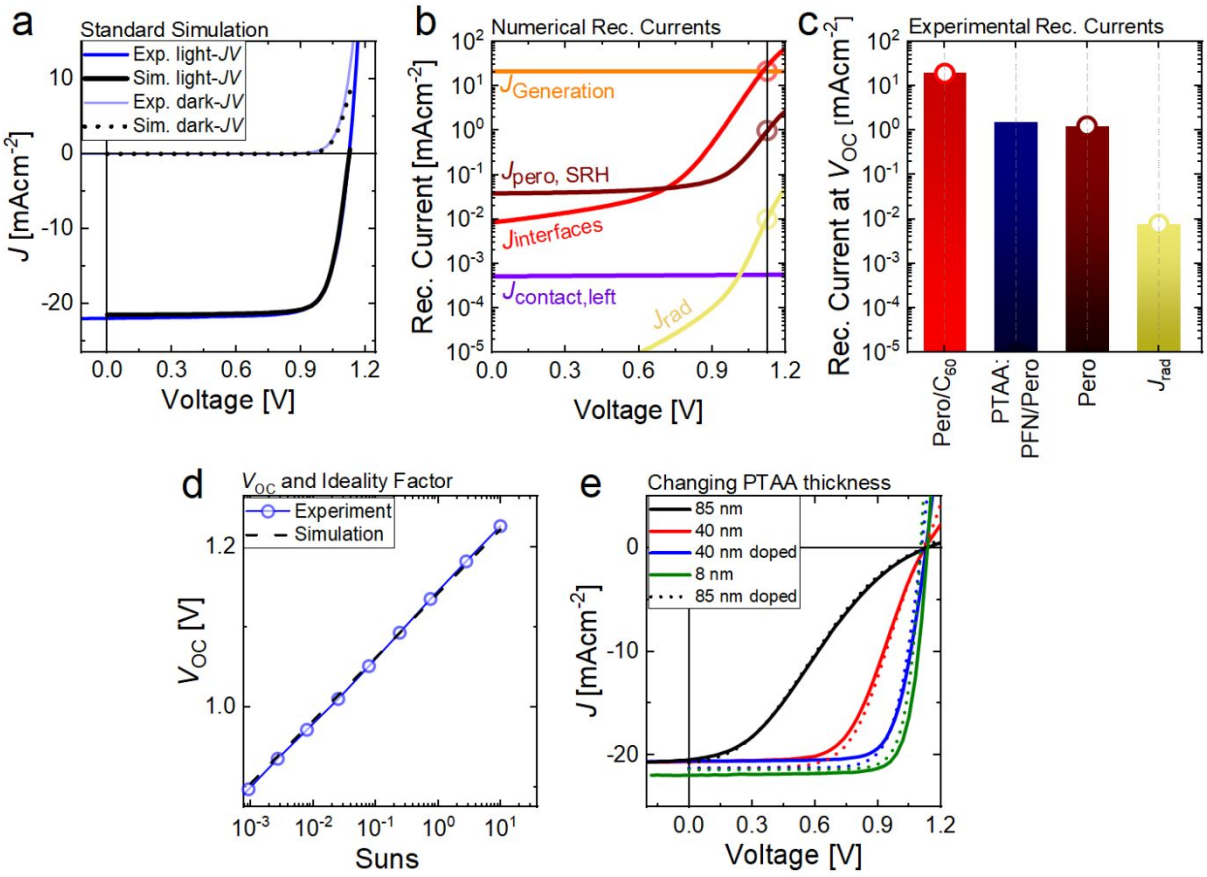

Supplementary Figure S1. ***(a)*** *Numerically modelled and experimental JV-curves of p-i-n type triple cation perovskite solar cells based on a 8 nm thick PTAA bottom layer. The interfacial recombination velocities and bulk lifetimes were obtained using transient photoluminescence measurements.*[1] ***(b)*** *Simulated voltage dependent non-radiative recombination currents at the interfaces and in the neat material compared to radiative recombination in the bulk and the generation current. Interfacial recombination outweighs Shockley-Read-Hall recombination in the neat material by roughly one order of magnitude. The numerically modelled recombination currents match the experimentally measured recombination currents under open-circuit (V_{OC}) conditions which were obtained using steady-state PL measurements* ***(c)***.[2] ***(d)*** *The simulated intensity dependent V_{OC} demonstrates an identical ideality factor than obtained experimentally (n_{ID}~1.35).*[3] ***(e)*** *The simulations allow to fit the JV-curves of the cells with varying PTAA layer thickness as shown in this work.*

Supplementary Note 1

We note that **equation 1** is a simplification of Würfel's generalized Planck law which is only valid for quasi-Fermi level splittings that are a few $k_{\mathrm{B}}T$ smaller that the bandgap $\mu < E_{\mathrm{G}} - 3k_{\mathrm{B}}T$.[4] Moreover 2 conditions must be fulfilled: 1) J_{rad} and $J_{0,\mathrm{rad}}$ must have the same spectral dependence which means that recombination goes through the same recombination channels regardless of the QFLS. 2) The emission must come from free charges only and not from strongly bound excitons as only free charges create a QFLS. Both conditions are usually justified for perovskite cells.

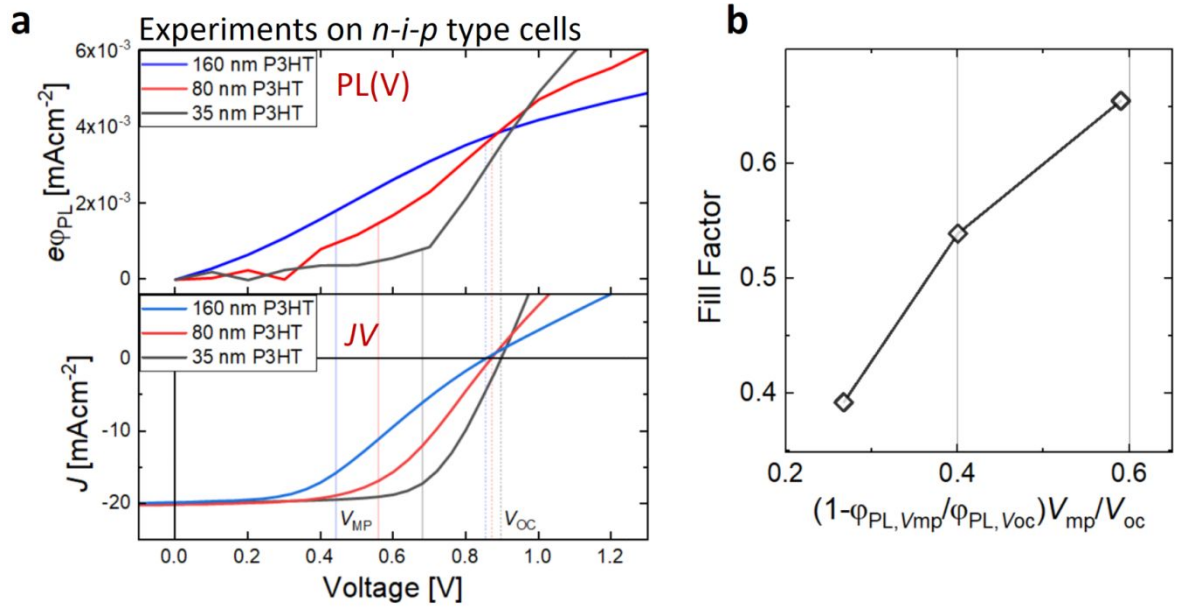

Supplementary Figure S2. ***(a)*** *Voltage dependent photoluminescence and corresponding JV-curves of n-i-p cells with the following structure: ITO/PEIE/C_{60}/triple cation perovskite/P3HT/MoO_3/Ag.* ***(b)*** *The device fill factor vs. the proposed figure of merit from the voltage dependent PL (1 minus the PL quenching ratio from V_{OC} to V_{MP} times V_{MP}/V_{OC}). The results confirm the trends observed for p-i-n type PTAA-based cells shown in the main text.*

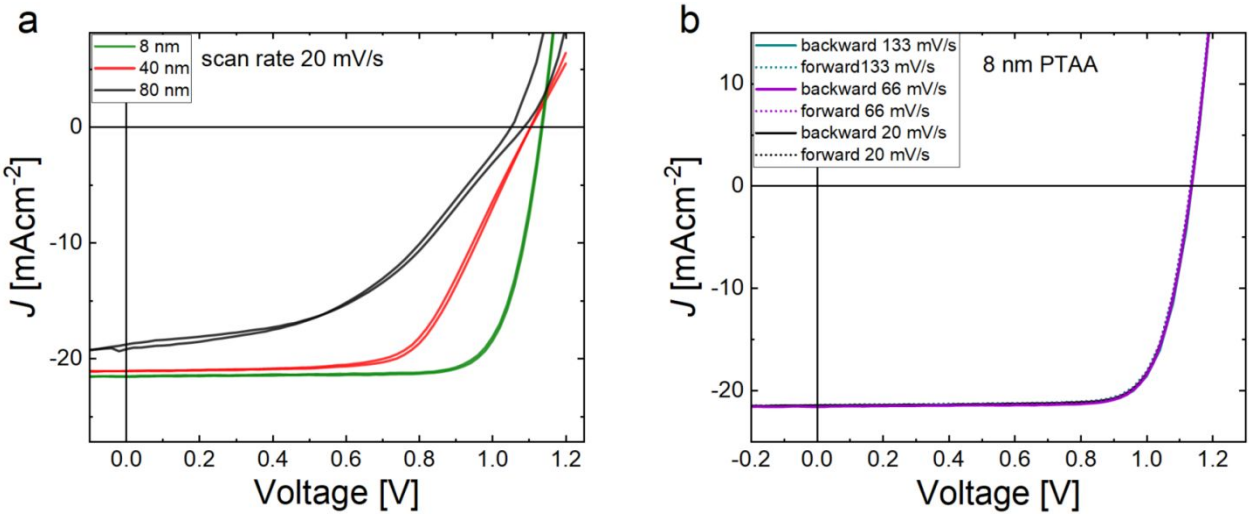

Supplementary Figure S3. ***(a)*** *Hysteresis scans on devices with different PTAA layer thicknesses at a comparatively slow scan rate which is comparable to the voltage dependent PL scan rate demonstrating a small hysteresis in the power generating JV regime.* ***(b)*** *The effect of the scan rate is further demonstrated for the device with 8 nm which highlights a negligible hysteresis within the studied time-range.*

Supplementary References

(1) Stolterfoht, M.; Wolff, C. M.; Márquez, J. A.; Zhang, S.; Hages, C. J.; Rothhardt, D.; Albrecht, S.; Burn, P. L.; Meredith, P.; Unold, T.; et al. Visualization and Suppression of Interfacial

Recombination for High-Efficiency Large-Area Pin Perovskite Solar Cells. *Nat. Energy* **2018**, *3* (10), 847–854.

(2) Stolterfoht, M.; Caprioglio, P.; Wolff, C. M.; Márquez, J. A.; Nordmann, J.; Zhang, S.; Rothhardt, D.; Hörmann, U.; Amir, Y.; Redinger, A.; et al. The Impact of Energy Alignment and Interfacial Recombination on the Internal and External Open-Circuit Voltage of Perovskite Solar Cells. *Energy Environ. Sci.* **2019**, *12* (9), 2778–2788.

(3) Caprioglio, P.; Stolterfoht, M.; Wolff, C. M.; Unold, T.; Rech, B.; Albrecht, S.; Neher, D. On the Relation between the Open-Circuit Voltage and Quasi-Fermi Level Splitting in Efficient Perovskite Solar Cells. *Adv. Energy Mater.* **2019**, *9* (33), 1901631.

(4) Würfel, P.; Würfel, U. *Physics of Solar Cells: From Basic Principles to Advanced Concepts*, 2nd Edition; Wiley-VCH: Weinheim, 2009.